coatings

MDPI

Article

Investigation of the Tribological Properties and Corrosion Resistance of Multilayer Si-DLC Films on the Inner Surfaces of N80 Steel Pipes

Shaolong Wang [1,*], Guangan Zhang [2], Anqing Fu [1], Xueqian Cao [2], Chengxian Yin [1] and Zhengyu Liu [2]

[1] Tubular Goods Research Institute of CNPC, Xi'an 710077, China; yincx@cnpc.com.cn (C.Y.)
[2] State Key Laboratory of Solid Lubrication, Lanzhou Institute of Chemical Physics, Chinese Academy of Sciences, Lanzhou 730000, China
* Correspondence: sk_0522@sina.com

Abstract: In order to solve the problem of the corrosion and wear of N80 metal pipelines exposed to corrosive media and abrasive sand during the development of petroleum resources, the proposed solution involves utilizing HC-PECVD technology to deposit a series of multilayer Si-DLC films with varying thicknesses on the inner surfaces of the N80 steel pipes. This investigation systematically explored the microstructure, mechanical properties, tribological features, and corrosion resistance of the multilayer Si-DLC films. Remarkably, after coating the multilayer $(Si\text{-}DLC)_{40}$ film on the inner wall of the N80 tube, the friction coefficient decreased from 0.7~0.75 to 0.2~3, and the wear rate decreased by two orders of magnitude. In addition, the corrosion current decreased by 50%, and the impedance doubled in a 3.5 wt% NaCl solution saturated with CO_2. Thus, the multilayer $(Si\text{-}DLC)_{40}$ film on the inner wall of the N80 tube exhibited superior tribological properties and exceptional corrosion resistance. These findings are anticipated to furnish valuable data and technical insights for mitigating corrosion in N80 steel pipes during petroleum exploitation.

Keywords: petroleum exploitation; Si-DLC film; CO_2; corrosion resistance; tribology properties

Citation: Wang, S.; Zhang, G.; Fu, A.; Cao, X.; Yin, C.; Liu, Z. Investigation of the Tribological Properties and Corrosion Resistance of Multilayer Si-DLC Films on the Inner Surfaces of N80 Steel Pipes. *Coatings* **2024**, *14*, 385. https://doi.org/10.3390/coatings14040385

Academic Editor: Michał Kulka

Received: 16 January 2024
Revised: 19 March 2024
Accepted: 20 March 2024
Published: 25 March 2024

1. Introduction

As the global economy advances, the demand for petroleum, natural gas, and other energy in various countries continues to increase, leading to ongoing enhancements in both the volume and efficiency of petroleum and gas exploitation. Carbon dioxide flooding technology is one of the technologies with high efficiency in petroleum recovery [1]. However, the application of carbon dioxide flooding technology often subjects the petroleum production pipeline to prolonged exposure to high-temperature and high-pressure CO_2 environments. Furthermore, the synergistic effect between CO_2 and the formation water, containing high Cl^- and other corrosive media, leads to accelerated pipeline corrosion during petroleum exploitation [2]. This corrosion risk poses a potential threat to pipeline perforation, failures, petroleum leakage, and safety incidents. Given the above situation, researchers have proposed several conventional solutions, such as high-corrosion-resistant alloys, corrosion inhibitors, lubricating greases, and cathodic protection. While high-corrosion-resistant alloy pipelines meet industrial requirements, their high cost makes them unsuitable for large-scale production applications, limiting their use in specific environments [3]. Corrosion inhibitors, lubricating greases, and cathodic protection methods all necessitate regular maintenance, thereby increasing the operational cost and demanding specific process operations.

From the perspective of the economy and environment, the most effective measure is to employ physical or chemical methods to create a modified layer with enhanced corrosion resistance on the inner surfaces of metal pipelines. This approach can effectively

decelerate the corrosion of petroleum and gas during production and transportation. Fayyad et al. [4,5] deposited a chemical Ni-P film on the surface of API X100/X120 steel pipelines to improve the corrosion and wear properties of materials. The Ni-P film exhibits superior corrosion resistance, attributed to the formation of hypophosphite ions in an acidic environment. Although the Ni-P film does not completely prevent the penetration of corrosive media, it significantly retards the corrosion rate of the metal, playing a substantial role in protecting metal pipelines. Wang et al. [6] used a high-power diode laser to prepare a Ni-Cr-Mo film on an X70 steel substrate and studied its corrosion behavior in simulated H_2S and CO_2 solutions. The morphology of the Ni-Cr-Mo film did not significantly change before and after the corrosion experiment, showing a stable anti-corrosion performance. The hard W-C system deposit prepared by Dushik et al. [7] through chemical vapor deposition technology is also considered a promising anti-corrosion film because of its extremely low porosity of 0.02% and outstanding corrosion resistance.

One of the most efficient ways to increase the corrosion resistance of the inner surfaces of metal pipes is to use hollow-cathode plasma-enhanced chemical vapor deposition (HC-PECVD) technology to deposit diamond-like carbon (DLC) films. DLC films exhibit high hardness, excellent chemical inertness, and no chemical reactions with acid and alkali salts [8–13]. By customizing the adhesion to substrates and depositing multiple layers, M. J. Hoque et al. [8] created a flawless F-DLC film with minimal surface energy and a Young's modulus akin metals. In a three-year trial involving steam condensation, the F-DLC film retained its hydrophobic properties, leading to continued and enhanced dropwise condensation on various metal substrates.

Applying an acid treatment to DLC surfaces enhances their hydrophilicity, while XPS analysis revealed a 50% rise in ArmeenT uptake post-treatment, leading to reduced friction in micro-scale friction tests [9]. In a plasma immersion ion implantation and deposition (PIII&D) process, the inner surface of a narrow steel tube was coated with a substantial layer of graphene-like (Gr-like) material [10]. The study reported by Brown et al. [11] presented a superhydrophobic duplex coating system, demonstrating sustained water droplet mobility after 170 icing/deicing cycles, resilience to extended UV and high-temperature exposure, and a 300-fold enhancement compared with stearic acid in rain erosion resistance tests. Ellis et al. [12] prepared DLC films on the inner surfaces of pipes in a test conducted in a high-temperature and high-pressure autoclave simulating the acid production environment. Remarkably, even when intentionally mechanically damaged before the test, the film demonstrated resilience against chemical attacks. The investigation reported by Koshigan et al. [13] showed that environmental factors significantly affect the formation and release of adhesive junctions between steel and a-C:H:Si:O, with oxygen (p > 10 mbar) or hydrogen (p > 50 mbar) promoting bond detachment during sliding. In recent years, Zhang's group used an alternating multilayer design of a compressive stress layer (Si-poor layer) and a tensile stress layer (rich–poor layer) to reduce the residual stress in DLC films, thus successfully preparing multilayer thick DLC films exceeding 50 μm in thickness [14]. They also deposited these thick DLC films on the inner surfaces of various materials, including 304 stainless steel pipes, aluminum pipes, and cast iron, with different diameters and shapes, such as straight pipes, bent pipes, and U-shaped pipes [15,16]. After undergoing 480 h and 720 h neutral salt spray tests, the film surfaces displayed no noticeable damage, indicating exceptional corrosion resistance and a prolonged service life [17,18]. In summary, Zhang's group systematically studied the feasibility of the uniform deposition of anti-corrosion and wear-resistant integrated DLC films on the inner surfaces of metal pipes, the universality of deposition technology, the influence and optimization of doping on the performance of DLC films, and the functionalization of DLC films. Therefore, it is highly anticipated to use HC-PECVD technology to prepare DLC films on the inner walls of N80 tubes. A PECVD-deposited Si/Si-DLC/DLC coating inside a high-aspect-ratio pipe exhibited optimal performance at 70 mTorr, with an increased thickness, superior hardness (18.11 GPa), a low friction coefficient (0.12), a minimal wear rate (7.37×10^{-9} mm^3/Nm), and strong adhesion (32 N), making it ideal for

pipeline protection [19]. The research results of Mariano et al. [10] indicated that the plasma immersion ion implantation and deposition (PIII&D) process coated a narrow steel tube with a thick, well-aligned multilayer graphene film, exhibiting a cauliflower-like structure. Local gas feeding enabled an efficient carbon species supply, expanding PIII&D's utility for diverse applications. The research results of Xu et al. [20] indicate that enhanced glow discharge–plasma immersion ion implantation and deposition (EGD-PIII&D) achieves a deposition rate of 1.3 μm/min for DLC films on quartz tubes. Carbon films deposited inside titanium alloy tubes via PIII&D enhance corrosion resistance, as reported by Santos et al. [21], extending the tube lifespan in satellite propulsion and thermal control systems by inhibiting corrosive species permeation.

In the development of petroleum resources, widely used N80 metal pipes are prone to corrosion and wear under the action of corrosive media and abrasive sand. Therefore, a series of multilayer Si-DLC films with different thicknesses were prepared on the inner surfaces of N80 steel pipes with inner diameters of 75 mm by HC-PECVD technology. The microstructures, mechanical properties, tribological behaviors, and corrosion resistance of the Si-DLC films were systematically studied. The novelty of this article lies in the preparation of high hardness and adhesion on the inner walls of pipelines with poor surface quality, such as high surface roughness and possible partial oxidation, using multilayer $(Si\text{-}DLC)_{40}$ films with excellent tribological and corrosion resistance properties on the inner walls of N80 steel pipes. This has great practical significance for improving the service performance and lifespan of N80 metal pipes.

2. Experimental Details

2.1. Preparation of Multilayer Si-DLC Films on the Inner Surfaces of N80 Steel Pipes

Multilayer Si-DLC films with 10, 20, and 40 cycles were prepared with N80 pipes with a diameter of 75 mm by the HC-PECVD technique. The diagram of the hollow cathode coating system is shown in Figure 1. The heat treatment state of the N80 pipes was normalized (N). The chemical composition of the N80 pipes was mainly composed of elements such as C, Si, Mn, P, S, etc. The metallographic structure of the N80 pipes was pearlite P+ferrite F with a grain size of 9.0. Firstly, the N80 steel pipes were mechanically polished via sand-blasting and a grinding wheel. Secondly, an ultrasonic cleaner was used to clean the N80 steel pipes immersed in acetone and anhydrous ethanol for 20 min in turn, and then they were dried with nitrogen.

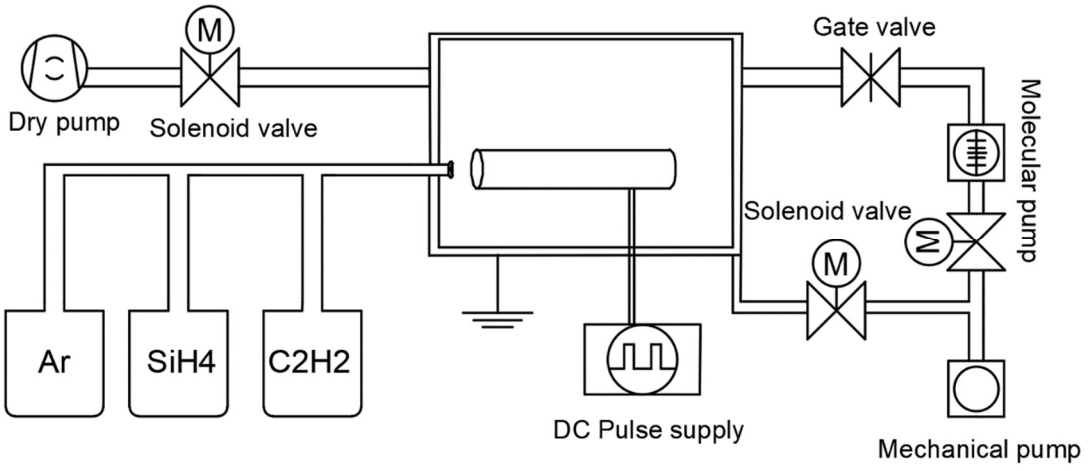

Figure 1. The diagram of the hollow cathode coating system.

The detailed steps for depositing DLC are shown in Table 1. (1) Clean the surface of the sample by Ar^+ bombardment: when the vacuum chamber pressure is maintained at 1.5×10^{-3} Pa, inject high-purity argon until the air pressure in the vacuum chamber is 5 Pa,

the pulse bias voltage is −6 kV, the duty cycle is 30%, and the cleaning time is 30 min. (2) Deposit the silicon interlayer: introduce two precursor gases (silane and argon), and deposit the silicon transition layer for 20 min under the conditions of a 15.0 Pa pressure, a −15 kV pulse bias voltage, and a 30% duty cycle. (3) Prepare the multilayer film: Use the mixture of argon, acetylene, and silane as the element source and keep the pulse bias voltage of the substrate within −0.65~−0.8 kV and the pulse duty ratio as 15%~20%. The multilayer Si-DLC films with 10, 20, and 40 cycles have 10, 20, and 40 Si-poor DLC layers and 10, 20, and 40 Si-rich DLC layers, respectively. As shown in Table 2, the C/Si ratio content in the Si-poor layer and the Si-rich thin layer are approximately 82/7 and 74/15, respectively [14]. It is noted that the thickness of the individual layers gradually changes as growth proceeds, becoming thinner as the number of periods increases. Their thicknesses are 4.1, 7.6, and 10.2 μm, respectively. Finally, take out the samples from the vacuum chamber after it is cooled to room temperature. Table 1 displays the detailed process parameters.

Table 1. Parameters for deposition of multilayer Si-DLC films on N80 steel pipes.

Process Step	Precursors	Pressure (Pa)	Voltage (V)	Time (min)
Cleaning	Ar	5	−6000	30
Adhesion	SiH_4 + Ar	15	−15,000	20
Si_x-DLC	C_2H_2 + SiH_4 + Ar	18–20	−650~−800	4.5
Si_y-DLC		11–13	−650~−800	1.5

Table 2. Percentage contents of C, Si, and O atoms in the individual layers [14].

Sample	Concentration (at.%)		
	C	Si	O
Si-poor DLC layer	82.34	7.14	10.52
Si-rich DLC layer	74.49	14.79	10.73

2.2. Characterization of Structure and Mechanical Properties of Multilayer Si-DLC Films

The cross-sectional structures and thicknesses of the multilayer Si-DLC films were obtained by field-emission scanning electron microscope (FESEM, JSM-6701F, JEOL, Tokyo, Japan). The surface morphologies and roughness of the multilayer Si-DLC films were evaluated by using a 3D profilometer (Micro Xam-800, KLATencor, Milpitas, CA, USA). The bonding structures of the films were analyzed by a Raman spectrometer (LabRam HR Evolution, Renishaw, Wotton-under-Edge, UK) with a laser wavelength of 532 nm, and the signal collection range was 800~2000 cm^{-1}. A nanoindenter (TTX-NHT2, Anton Paar, Graz, Austria) was used to test the hardness and elasticity. The Berkovich diamond indenter was unloaded after a fixed load was applied, and the press–unload curve was obtained. Therein, 30 mN and 10 s were taken as the maximum load and loading time. The indentation depth was within one-tenth of the thickness of the multilayer Si-DLC film to avoid the influence of the substrate on the measurement results.

2.3. Evaluation of Tribological and Corrosion Properties of Multilayer Si-DLC Films

A CSM (Tribo-S-D-0000, Anton Paar, Graz, Austria) friction and wear tester was used to evaluate the tribological properties of the multilayer Si-DLC films in an atmospheric environment (25 °C; 35% RH). Therein, a GCr15 ball with a diameter of 6 mm was selected as the counterpart, and the tribological behaviors were examined under the conditions of 5 N, 5 Hz, 5 mm, and 20,000 cycles. Before the friction test, the multilayer Si-DLC films and GCr15 balls were cleaned by ultrasonic cleaning in acetone and ethanol for 10 min, in turn, to remove surface contaminants and dried with dry nitrogen. The corrosion resistance of the films was evaluated using the electrochemical workstation (PGSTAT302,

Metrohm Autolab, Utrecht, The Netherlands). The corrosion performance test adopted a three-electrode system, in which a saturated calomel electrode, a platinum plate, and the film were the reference electrode, the opposite electrode, and the working electrode, respectively. The corrosion medium was a 3.5 wt% NaCl solution and a 3.5% NaCl solution saturated with CO_2. Before the electrochemical measurements, the multilayer Si-DLC films were immersed in the corrosion medium for 40 min to stabilize the open circuit potential of the samples, and 10 mV/s was selected as the scanning speed of the potentiodynamic polarization test. The electrochemical impedance spectrum test frequency range was 100 kHz~10 MHz, and the disturbance amplitude was 10 mV. We repeated the tribological and corrosion tests at least three times to ensure the reliability of the results.

3. Results and Discussion

3.1. Microstructures and Surface Morphologies of Multilayer Si-DLC Films on the Inner Surfaces of N80 Steel Pipes

Figure 2 depicts a photo of the N80 steel pipe coated with the multilayer $(Si\text{-}DLC)_{40}$ film. The macro-surface of the multi-layer Si-DLC film was smooth and dense. In Figure 3, the FESEM surface and cross-sectional image illustrate the multilayer (Si-DLC)40 film on the inner surface of the N80 steel pipe. The $(Si\text{-}DLC)_{40}$ film consisted of the Si transition layer and the $(Si\text{-}DLC)_{40}$ layer with different Si doping contents. By the high-energy implantation of Si ions on the N80 steel substrate, a transition layer was obtained with the proportion of silane/argon in the gas mixture as 2:1. The Si transition layer improved the interface matching between the $(Si\text{-}DLC)_{40}$ layer and the metal substrate, thus improving the film substrate's adhesive strength. The $(Si\text{-}DLC)_{40}$ film, consisting of a Si-poor DLC layer (Si_x-DLC) and a Si-rich DLC layer (Si_y-DLC), alternately, was deposited on the surface of the interlayer. For the Si-poor and Si-rich layers, the acetylene/silane/argon proportions in the Si-poor and Si-rich films were 2:1:3 and 2:1:1, respectively. The overall thickness of the multilayer $(Si\text{-}DLC)_{40}$ film was approximately 11.53 μm. Furthermore, the film exhibited density and uniformity without evident cracks, holes, or other defects, indicating excellent adhesive strength.

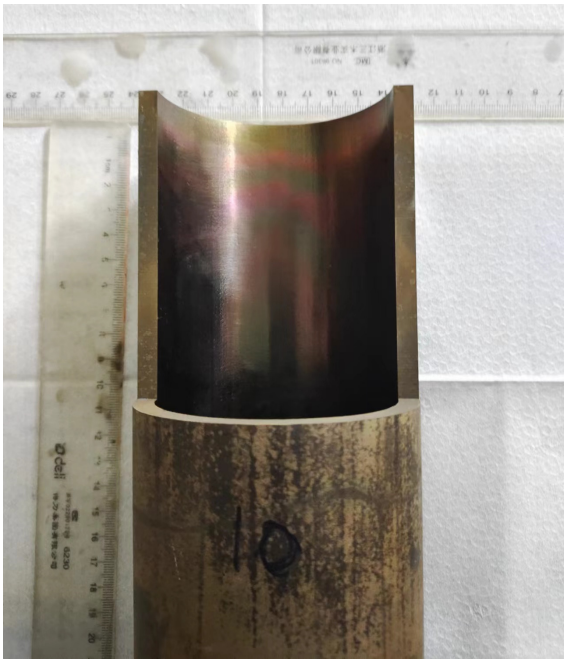

Figure 2. N80 steel pipe with DLC film.

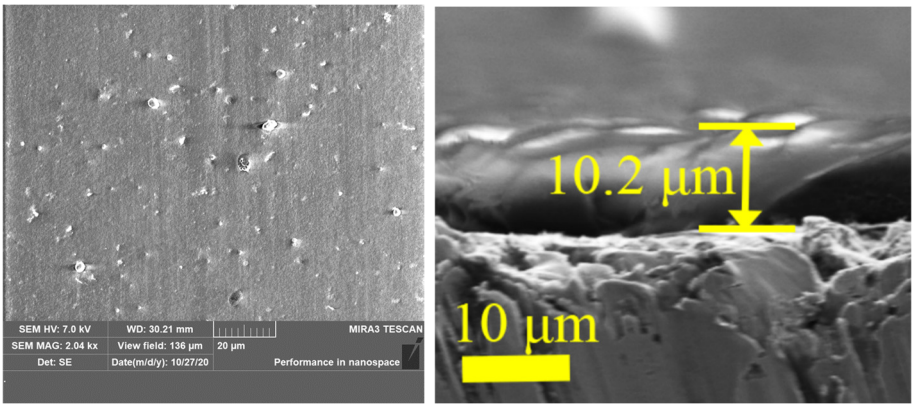

Figure 3. Surface and cross-sectional morphologies of $(Si\text{-}DLC)_{40}$ film on the inner surface of N80 steel pipe.

Figure 3 exhibits the Raman spectrum of the multilayer $(Si\text{-}DLC)_{40}$ film on the inner surface of the N80 steel pipe. The Raman peak of the DLC film in the range of 1000~1800 cm^{-1} was fitted to the D peak and G peak at about 1350 cm^{-1} and 1560 cm^{-1} by the Gaussian function, respectively [22–25]. The D peak was caused by the sp^2-C atom in the ring structure or cluster, and the G peak was caused by the sp^2-C structure in the chain or aromatic ring [21].

Figure 4 shows that the multilayer $(Si\text{-}DLC)_{40}$ film had an asymmetric wide peak in the range of 1000~1800 cm^{-1}, which is the Raman spectrum of a typical DLC film. The D peak and G peak fitted by the Gaussian function were located at 1334 cm^{-1} and 1513 cm^{-1}, respectively [26]. It was determined that the peak position migrated to a lower wavenumber compared with a pure DLC film. This was mainly due to two reasons. On the one hand, Si doping can promote the hybridization of sp^3 and inhibit the formation of sp^2 clusters [21,27]. On the other hand, Si doping into a multilayer $(Si\text{-}DLC)_{40}$ film reduces the internal stress [28]. The incorporation of larger Si atoms and weaker C-Si bonds diminishes the vibration frequency of the C=C bond, resulting in the migration of Raman peaks to the low-wavenumber region.

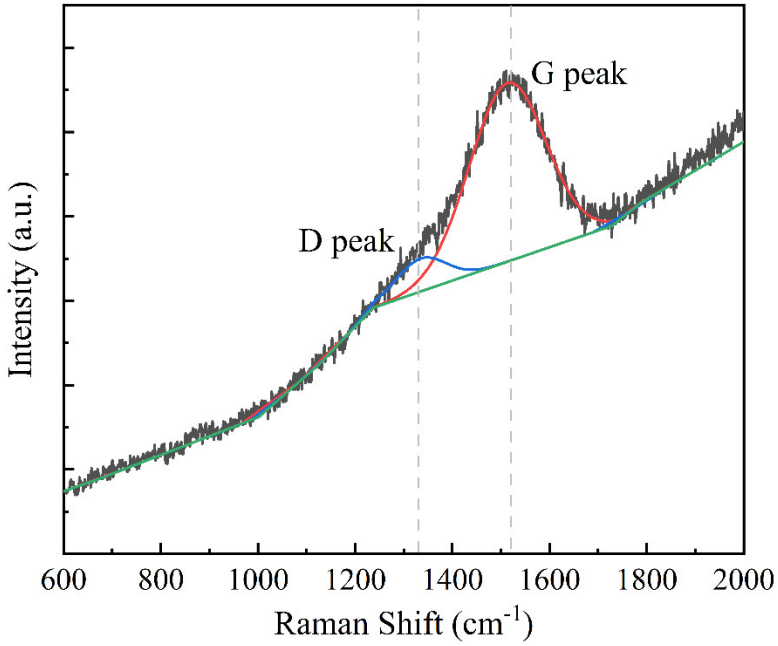

Figure 4. Raman spectrum of $(Si\text{-}DLC)_{40}$ film on the inner surface of N80 steel pipe.

To further analyze the surface element composition of the original film, XPS analysis was conducted, as shown in Figure 5. In the case of the multilayer films, as shown in Figure 5b, the C1s spectrum was fitted into four peaks by the Gaussian function, namely, the O-C=O bond at 288.0 eV, the C-O bond at 285.6 eV, the C-C bond at 284.3 eV, and the C-Si bond at 283.4 eV. In addition, Figure 5c,d further demonstrates the presence of C-O and C-Si bonds in the film. These results affirm the successful preparation of multilayer Si-DLC thin films through hollow-plasma chemical vapor deposition.

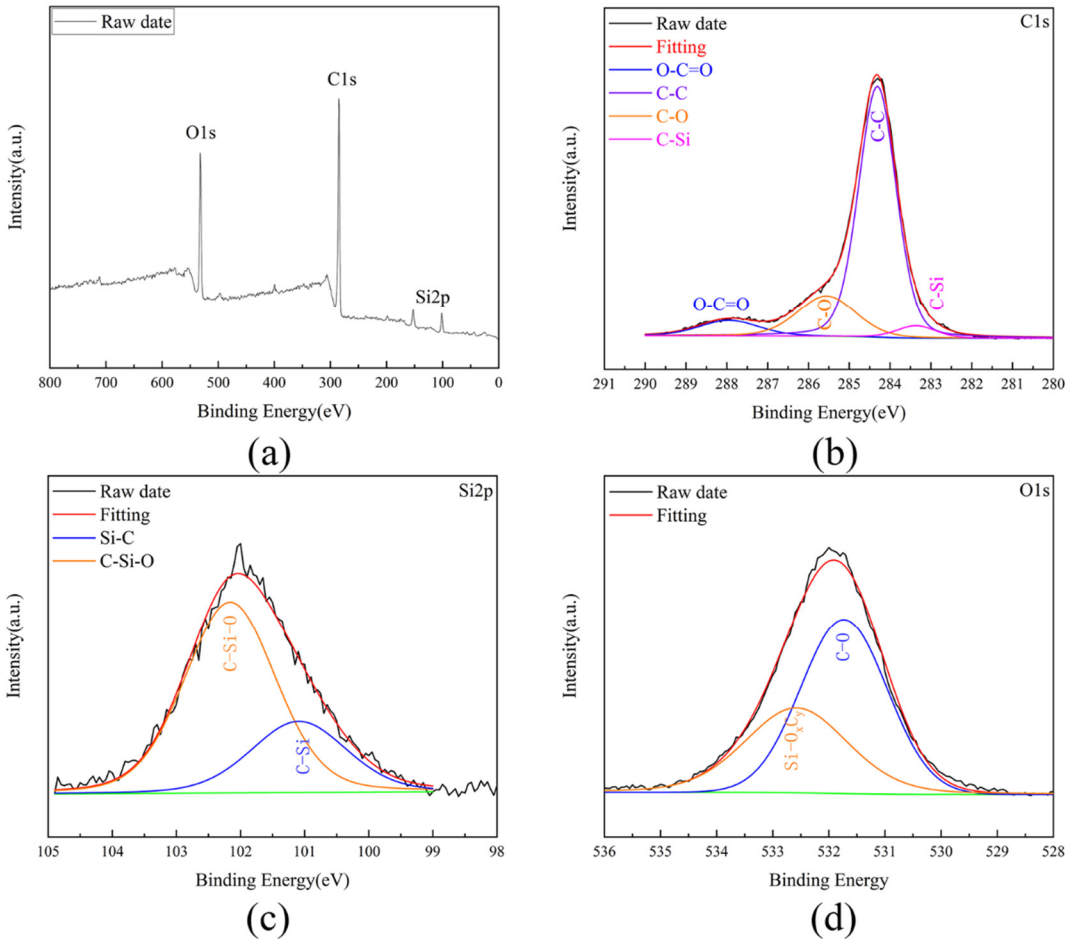

Figure 5. XPS diagrams of $(Si\text{-}DLC)_{40}$ film on the inner surface of N80 steel pipe: (**a**) full spectrum, (**b**) C1s spectrum, (**c**) Si2p spectrum, (**d**) O1s spectrum.

3.2. Mechanical Properties of the Films on the Inner Surfaces of N80 Steel Pipes

The load–displacement curve of the multilayer $(Si\text{-}DLC)_{40}$ film on the N80 steel pipe is shown in Figure 6. As the thickness of the multilayer film increased, both the hardness and adhesion showed an upward trend. This is consistent with our previous research findings [14]. The $(Si\text{-}DLC)_{40}$ film exhibited the best mechanical properties, with hardness and elastic moduli of 14.3 GPa and 115.7 GPa, respectively. It is important to study the adhesion of the $(Si\text{-}DLC)_{40}$ film in tribology and corrosion resistance applications because the film may peel off from the substrate under external normal and shear forces [29].

The scratch image is shown in Figure 7. At the initial stage of sliding, the film exhibited plastic deformation characteristics. With the increase in the load, the transverse cracks began to appear on the film's surface, indicating that the film was beginning to fail and, at this point, was called Lc1, representing the initial peeling point of the film. Subsequently, as the load continued to rise, continuous transverse cracks developed, indicating the onset of continuous spalling phenomena. This stage, marked as Lc2, represented the

point of continuous spalling. As the thickness of the film increased, the adhesion of the film also increased. The Lc1 and Lc2 of the $(Si\text{-}DLC)_{40}$ film were 6.8 N and 14.2 N, respectively. By reducing the mismatch between the multilayer $(Si\text{-}DLC)_{40}$ film and the N80 steel substrate, the interface stress was greatly reduced, thus improving the adhesion of the multilayer $(Si\text{-}DLC)_{40}$ film [29].

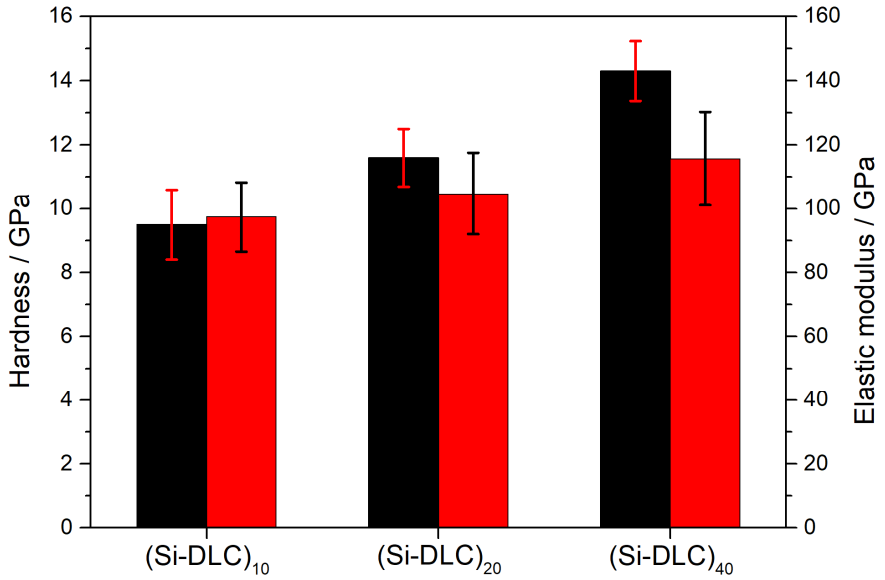

Figure 6. Mechanical properties of nanoindentation multilayer Si-DLC film on the inner surface of N80 steel pipe: black column - Hardness, red column - Elastic modulus.

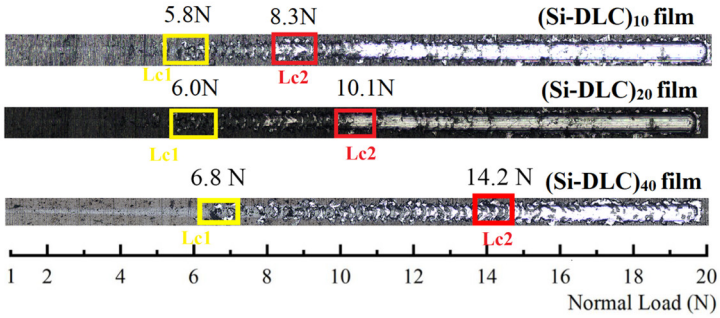

Figure 7. Scratch image of Si-DLC film on the inner surface of the N80 steel pipe.

3.3. Tribological Properties of Si-DLC Films on the Inner Surface of N80 Steel Pipe

Figure 8 shows the tribological properties of the N80 steel pipe and Si-DLC films in an atmospheric environment. In Figure 8a, the stable friction coefficients of the Si-DLC films are significantly lower than that of N80. The N80 steel pipe exhibits a low initial friction coefficient, followed by a rapid increase. Beyond 2000 revolutions, the friction coefficient fluctuates within the range of 0.7~0.75. Conversely, the friction curve for the $(Si\text{-}DLC)_{10}$ film stabilizes with minimal fluctuations beyond 6000 revolutions, maintaining a stable friction coefficient of about 0.4. The $(Si\text{-}DLC)_{20}$ film displays a relatively fluctuating friction coefficient, approximately at 0.22, while the $(Si\text{-}DLC)_{40}$ film's friction coefficient is also fluctuating, with a mean coefficient of friction (COF) of around 0.23. The friction coefficient curves all show a certain degree of fluctuation, mainly attributed to the higher roughness of the inner wall of the N80 pipe, and more abrasive particles appear as the friction increases. Figure 8b shows that the Si-DLC films significantly increased the wear resistance of the inner surface of the N80 steel pipe. As shown in Table 3, the wear rates of the N80 steel pipe, $(Si\text{-}DLC)_{10}$ film, $(Si\text{-}DLC)_{20}$ film, and $(Si\text{-}DLC)_{40}$ film were 2.3×10^{-4}

mm³·N⁻¹·m⁻¹, 3.8 × 10⁻⁶ mm³·N⁻¹·m⁻¹, 1.3 × 10⁻⁶ mm³·N⁻¹·m⁻¹, and 6.8 × 10⁻⁷ mm³·N⁻¹·m⁻¹, respectively.

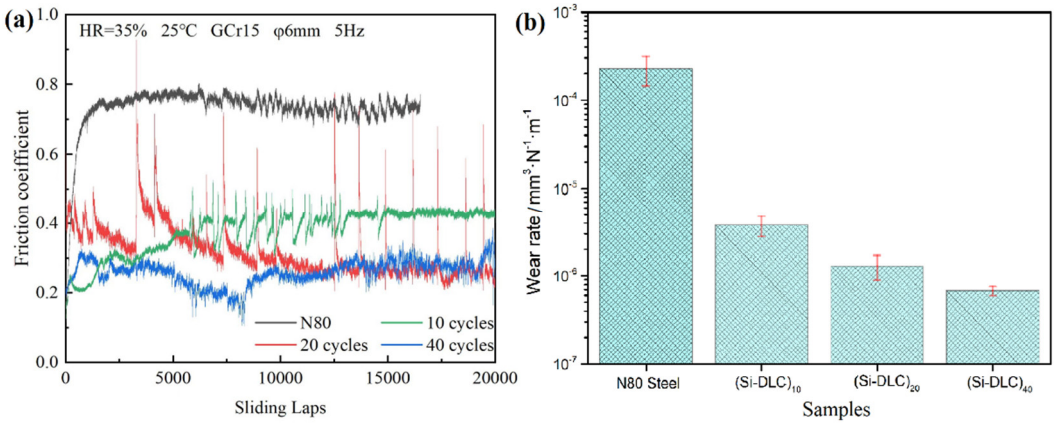

Figure 8. Friction curves (**a**) and wear rates (**b**) of the N80 steel pipe and Si-DLC films in an open-air environment.

Table 3. Friction coefficients and wear rates of N80 pipeline steel and multilayer Si-DLC films.

Sample	Friction Coefficient	Wear Rate/mm³·N⁻¹·m⁻¹
N80	~0.75	2.3 × 10⁻⁴
(Si-DLC)10	~0.4	3.8 × 10⁻⁶
(Si-DLC)20	~0.21	1.3 × 10⁻⁶
(Si-DLC)40	~0.23	6.8 × 10⁻⁷

Figure 9 shows the SEM images of the GCr15 steel ball wear scar and $(Si\text{-}DLC)_{40}$ film wear track. The formation of a transfer film in the wear scar is observed in the GCr15 steel ball wear scar, which is conducive to reducing the friction coefficient [30]. The internal surface of the $(Si\text{-}DLC)_{40}$ film wear track remains relatively smooth, and the original micro-pits of the film can still be observed, indicating excellent wear resistance. In addition, the evident furrows on the internal surface of the GCr15 steel ball wear scar indicate abrasive wear during the friction process.

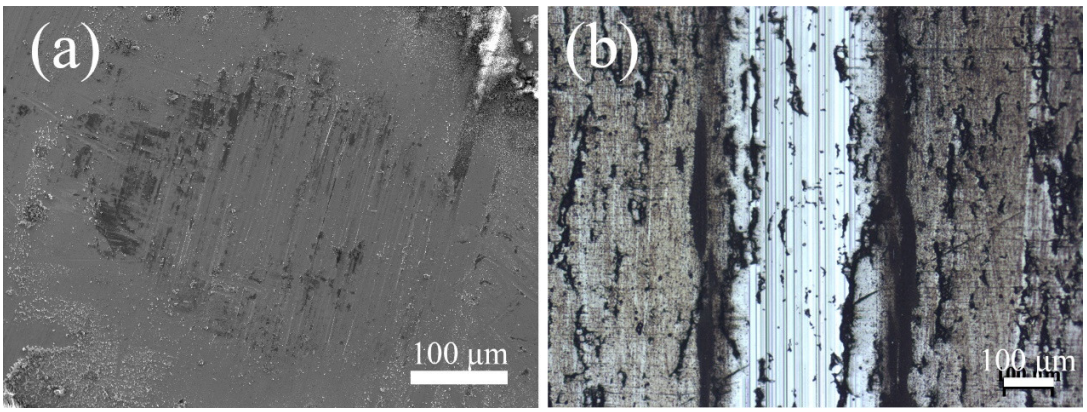

Figure 9. SEM images of (**a**) GCr15 steel ball wear scars and (**b**) $(Si\text{-}DLC)_{40}$ film wear track.

3.4. Corrosion Resistance of Si-DLC Films on the Inner Surface of N80 Steel Pipe

Figure 10a shows the potentiodynamic polarization curves of Si-DLC films. The potentiodynamic polarization diagrams were used to check the corrosion resistance. Table 4 summarizes the parameters calculated by the Tafel method. Stern–Geary Equations (1) and (2) were used to calculate R_p and porosity, respectively [31].

$$R_p = \frac{\beta_a \times \beta_c}{2.303 j_{corr}(\beta_a + \beta_c)} \quad (1)$$

β_a and β_c represent the Tafel slope of the anode and cathode, respectively, and j_{corr} is the corrosion current density of the N80 steel pipe and the Si-DLC film.

$$P = \frac{R_p(Substrate)}{R_p(film/substrate)} \times 10^{-|\Delta Ecorr/\beta a|} \quad (2)$$

$R_{p(substrate)}$ represents the Rp of the N80 steel pipe, $R_{p(film/substrate)}$ represents the R_p of the Si-DLC film, and ΔE_{corr} represents the E_{corr} difference between the N80 steel pipe and Si-DLC film. Generally, R_p indicates the difficulty of corrosion, and j_{corr} is related to the corrosion resistance of the material [32,33]. The incorporation of silicon into the DLC film facilitates the generation of silicon oxide on the film surface, leading to an improvement in the corrosion resistance. The corrosion ions can penetrate through the pores, so the film with lower porosity has good corrosion resistance [34]. It is seen in Table 4 that the Si-DLC film has a lower corrosion current density than that of the N80 steel pipe. Notably, the corrosion current density of the (Si-DLC)40 film is one-tenth of that of the N80 steel pipe, indicating that the $(Si\text{-}DLC)_{40}$ film effectively enhanced the corrosion resistance of the inner surface of the N80 steel pipe.

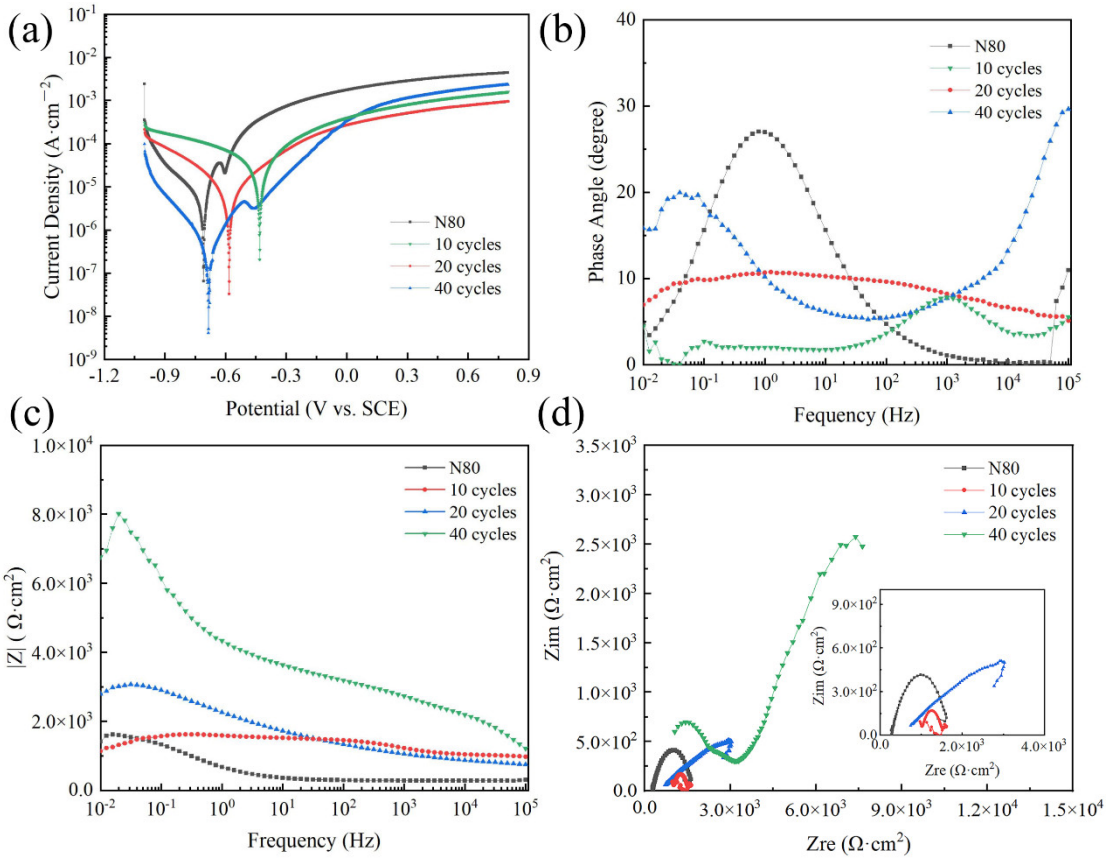

Figure 10. Potentiodynamic polarization curves (**a**), Bode diagrams (**b**,**c**), and Nyquist diagram (**d**) of the inner surface of N80 steel pipe and Si-DLC film.

Table 4. Polarization results of N80 steel pipe internal surface and Si-DLC film.

Sample	E_{corr} (V)	j_{corr} (A·cm²)	Rp (Ω·cm²)	P (Ω·cm²)
N80	−0.431	8.21×10^{-5}	1.85×10^{3}	—
10 cycles	−0.582	1.39×10^{-5}	2.21×10^{3}	3.09
20 cycles	−0.710	5.22×10^{-6}	4.46×10^{3}	2.85
40 cycles	−0.683	4.99×10^{-7}	7.51×10^{4}	0.89

Figure 10 also shows the EIS results of the N80 steel pipe and Si-DLC film, encompassing the (b) and (c) Bode plots, along with the (d) Nyquist plots. A wide time constant can be seen for the N80 steel pipe, indicating that a passive film was formed. The Bode diagram of the Si-DLC film shows low-frequency time constants and high-frequency time constants. The low-frequency impedances of the Si-DLC film surpass those of the N80 steel pipe, indicating superior corrosion resistance. It should be noted that the impedance value of the $(Si\text{-}DLC)_{40}$ film in Figure 10c reaches 8×10^3 Ω·cm², which is four times that of N80 steel pipe.

Figure 11 and Table 5 show the electrochemical test results of the inner surface of the N80 steel pipe and the $(Si\text{-}DLC)_{40}$ film. The E_{corr} of $(Si\text{-}DLC)_{40}$ film is slightly lower than that of N80. The corrosion current density of the $(Si\text{-}DLC)_{40}$ film is only half of that of the inner surface of the N80 steel pipe. The polarization resistance of the $(Si\text{-}DLC)_{40}$ film is about twice that of the inner surface of the N80 steel pipe, and the porosity is less than 5%. The above results show that the $(Si\text{-}DLC)_{40}$ film has better corrosion resistance than the N80 steel pipe, and the impedance value of the $(Si\text{-}DLC)_{40}$ film is higher than that of the N80 steel pipe.

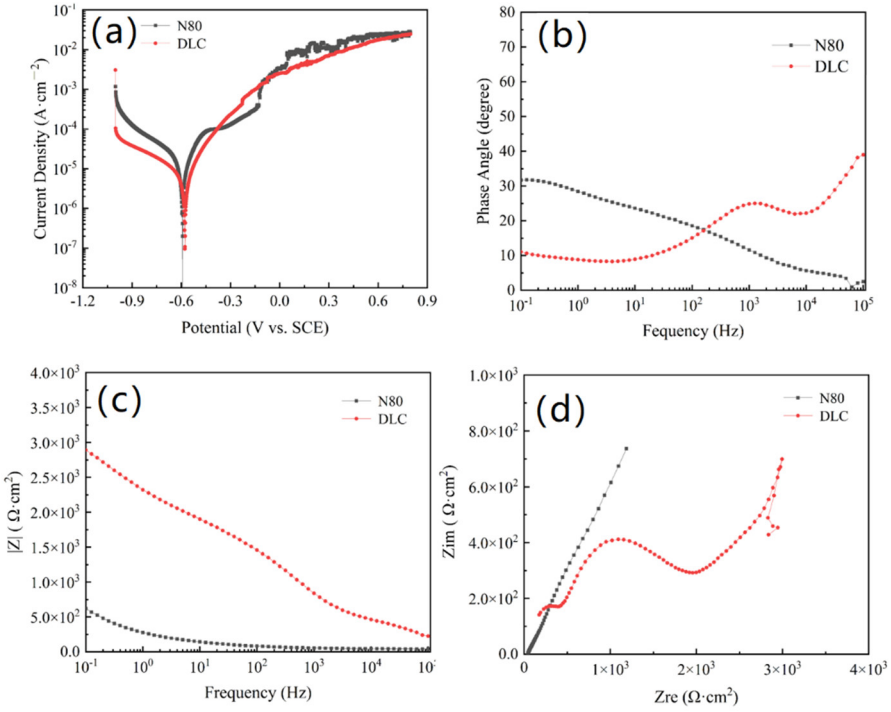

Figure 11. Potentiodynamic polarization curves (**a**), Bode diagrams (**b**,**c**), and Nyquist diagram (**d**) of N80 steel pipe inner surface and $(Si\text{-}DLC)_{40}$ film in 3.5% NaCl solution with saturated CO_2.

Table 5. Polarization results of N80 steel pipe internal surface and $(Si\text{-}DLC)_{40}$ film.

Sample	E_{corr} (V)	j_{corr} (A·cm²)	Rp (Ω·cm²)	P (Ω·cm²)
N80	−0.628	1.86×10^{-5}	3.12×10^3	—
Si-DLC	−0.604	7.67×10^{-6}	6.79×10^3	3.09

It is observed in Figure 12 that the surface of the $(Si\text{-}DLC)_{40}$ film was still smooth and flat without microscopic defects after the corrosion test. This indicates that the corrosive medium did not penetrate the passivation of the substrate surface, and only slight corrosion occurred on the surface of the thin film. Therefore, the $(Si\text{-}DLC)_{40}$ film provided good protection to the inner surface of the N80 steel pipe, as the corrosion resistance of the inner surface of the N80 steel pipe was significantly improved. Then, the surface of the wear track after the corrosion test was analyzed by X-ray photoelectron spectroscopy (XPS), as

shown in Figure 13. Through Gaussian fitting, the C1s peak could be decomposed into four peaks at 288.3 eV, 285.6 eV, 284.8 eV, and 284.5 eV, corresponding to the O-C=O bond, C-O bond, C-C bond, and C-Si bond, respectively [35,36]. After comparing with the original film, as depicted in Figure 5a, the content of the silicon–oxygen bond increased, indicating the formation of silicon oxide. Consequently, the corrosion resistance of the film was enhanced due to the formation of silicon oxide.

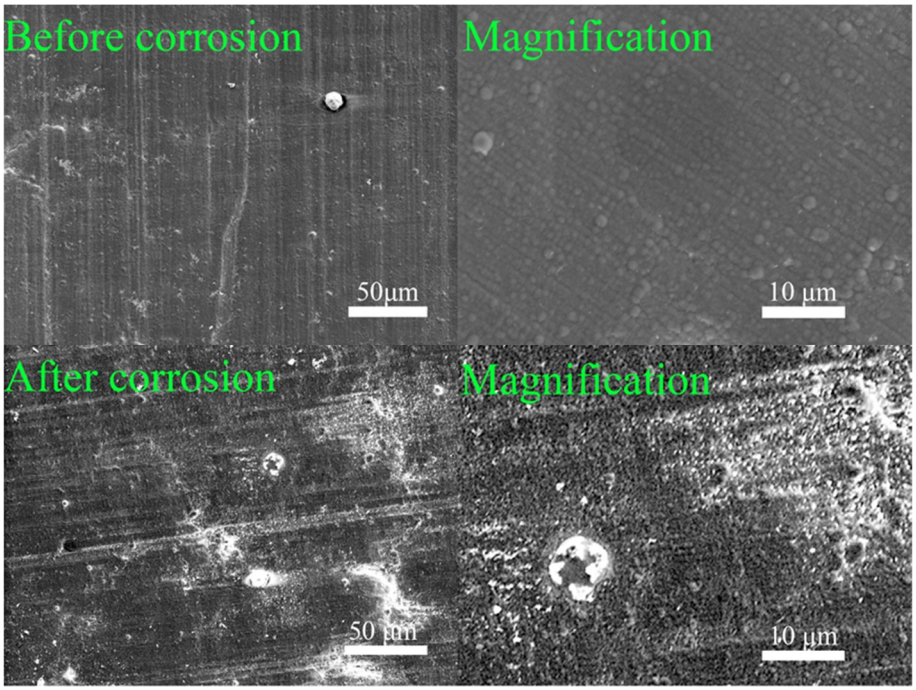

Figure 12. Surface morphology of $(Si\text{-}DLC)_{40}$ film after corrosion in 3.5% NaCl solution with saturated CO_2.

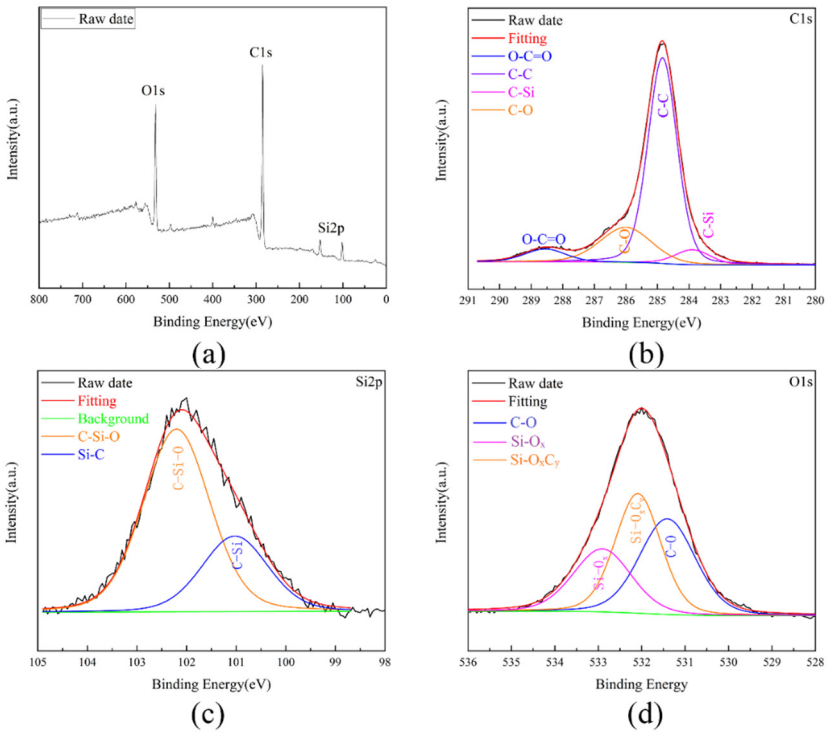

Figure 13. XPS image of $(Si\text{-}DLC)_{40}$ film after corrosion: (**a**) full spectrum, (**b**) C1s spectrum, (**c**) Si2p spectrum, (**d**) O1s spectrum.

4. Conclusions

(1) A series of multilayer Si-DLC films with 10, 20, and 40 modulation periods were successfully prepared on the inner surfaces of N80 steel pipes by hollow-cathode plasma-enhanced chemical vapor deposition technology. The multilayer $(Si\text{-}DLC)_{40}$ film exhibited a dense and uniform structure and the best mechanical performance, with a hardness of 14.3 GPa, an elastic modulus of 115.7 GPa, and an adhesive force Lc2 of 14.2 N.

(2) The tribological properties of the multilayer $(Si\text{-}DLC)_{40}$ film on the inner surfaces of N80 steel pipes surpassed those of uncoated N80 steel in atmospheric conditions. While the friction coefficient of uncoated N80 steel pipes ranged from 0.7 to 0.75, the multilayer $(Si\text{-}DLC)_{40}$ film demonstrated a significantly lower coefficient, approximately between 0.2 and 0.3. Moreover, the wear rate of the multilayer $(Si\text{-}DLC)_{40}$ film was three orders of magnitude lower than that of the N80 steel pipe. This was mainly attributed to the high mechanical and transfer film on the mating ball.

(3) The multilayer $(Si\text{-}DLC)_{40}$ film possessed more interfaces due to the increase in the film thickness, effectively prolonging the penetration distance of the corrosive medium in the 3.5 wt% NaCl solution and the 3.5 wt% NaCl solution saturated with CO_2. Therefore, the multilayer $(Si\text{-}DLC)_{40}$ film exhibited the best corrosion resistance and protective effect compared with the multilayer $(Si\text{-}DLC)_{10}$ and $(Si\text{-}DLC)_{20}$ films. In particular, the corrosion current density of the multilayer $(Si\text{-}DLC)_{40}$ film in the 3.5 wt% NaCl solution saturated with CO_2, approximately 7.67 $\mu A/cm^2$, was roughly half that of the N80 steel pipe, which recorded a corrosion current of about 18.6 $\mu A/cm^2$. Additionally, the impedance value of the multilayer $(Si\text{-}DLC)_{40}$ film (6790 $\Omega \cdot cm^2$) was approximately twice that of the uncoated N80 steel pipe (3120 $\Omega \cdot cm^2$).

Author Contributions: Methodology, G.Z., A.F., X.C., C.Y. and Z.L.; Formal analysis, X.C., C.Y. and Z.L.; Investigation, G.Z., A.F., C.Y. and Z.L.; Writing – original draft, S.W.; Writing – review & editing, S.W.; Project administration, S.W.; Funding acquisition, S.W. All authors have read and agreed to the published version of the manuscript.

Funding: This work was supported by the Basic Research and Strategic Reserve Technology Research Fund Project of the China National Petroleum Corporation (no. 2021DQ03(2022Z-01)).

Data Availability Statement: The data presented in this study are available on request from the corresponding author.

Conflicts of Interest: The authors declare no conflict of interest.

References

1. Safi, R.; Agarwal, R.K.; Banerjee, S.J.C.E.S. Numerical Simulation and Optimization of CO_2 Utilization for Enhanced Oil Recovery from Depleted Reservoirs. *Chem. Eng. Sci.* **2016**, *144*, 30–38.
2. Ma, W. Corrosion Behavior of Gas Storage Well Pipe Strings in Corrosive H_2S–CO_2 Environment. *J. Fail. Anal. Prev.* **2022**, *22*, 368–376.
3. Davoudi, M.; Heidari, Y.; Safadoost, A.; Samieirad, S. Chemical injection policy for internal corrosion prevention of South Pars sea-pipeline: A case study. *J. Nat. Gas Sci. Eng.* **2014**, *21*, 592–599.
4. Li, J.; Sun, C.; Roostaei, M.; Mahmoudi, M.; Fattahpour, V.; Zeng, H.; Luo, J.-L. Characterization and corrosion behavior of electroless Ni-Mo-P/Ni-P composite coating in CO_2/H_2S/Cl−brine: Effects of Mo addition and heat treatment. *Surf. Coat. Technol.* **2020**, *403*, 126416.
5. Sun, C.; Liu, S.; Li, J.; Zeng, H.; Luo, J.L. Insights into the Interfacial Process in Electroless Ni-P Coating on Supercritical CO_2 Transport Pipeline as Relevant to Carbon Capture and Storage. *ACS Appl. Mater. Interfaces* **2019**, *11*, 16243–16251.
6. Wang, Q.-Y.; Wang, X.-Z.; Luo, H.; Luo, J.-L. A study on corrosion behaviors of Ni–Cr–Mo laser coating, 316 stainless steel and X70 steel in simulated solutions with H_2S and CO_2. *Surf. Coat. Technol.* **2016**, *291*, 250–257.
7. Dushik, V.V.; Lakhotkin, Y.V.; Kuzmin, V.P.; Rozhanskii, N.V. The corrosion behavior of hard W–C system chemical vapor deposition layers in HCl and H_2S aqueous solutions. *Prot. Met. Phys. Chem. Surf.* **2017**, *52*, 1153–1156.
8. Hoque, M.J.; Li, L.; Ma, J.; Cha, H.; Sett, S.; Yan, X.; Rabbi, K.F.; Ho, J.Y. Ultra-resilient multi-layer fluorinated diamond like carbon hydrophobic surfaces. *Nat. Commun.* **2023**, *14*, 4902.
9. Khan, A.M.; He, X.; Wu, H.; Desanker, M.; Erdemir, A.; Chung, Y.W.; Wang, Q.J. Acid treatment of diamond-like carbon surfaces for enhanced adsorption of friction modifiers and friction performance. *Tribol. Lett.* **2018**, *66*, 128.

10. Mariano, S.D.F.M.; Silva, C.; Medeiros, F.I.D.; Pillaca, E.J.D.M.; Ueda, M. Graphene-like coated steel tube via biased hollow cathode discharges. *Vacuum* **2021**, *192*, 110431.
11. Brown, S.; Lengaigne, J.; Sharifi, N.; Pugh, M.; Moreau, C.; Dolatabadi, A.; Martinu, L.; Klemberg-Sapieha, J.E. Durability of superhydrophobic duplex coating systems for aerospace applications. *Surf. Coat. Technol.* **2020**, *401*, 126249.
12. Ellis, P.F.; Chambers, B.D. A diamond-like carbon pipe lining resistant to high temperature and pressure carbon dioxide/hydrogen sulfide environments. Paper presented at the CORROSION 2012, Salt Lake City, UT, USA, 11–15 March 2012; NACE-2012-1615.
13. Koshigan, K.D.; Mangolini, F.; McClimon, J.B.; Vacher, B.; Bec, S.; Carpick, R.W.; Fontaine, J. Understanding the hydrogen and oxygen gas pressure dependence of the tribological properties of silicon oxide-doped hydrogenated amorphous carbon coatings. *Carbon* **2015**, *93*, 851–860.
14. Wang, J.; Pu, J.; Zhang, G.; Wang, L. Interface Architecture for Superthick Carbon-Based Films toward Low Internal Stress and Ultrahigh Load-Bearing Capacity. *ACS Appl. Mater. Interfaces* **2013**, *5*, 5015−5024.
15. Wei, X.; Yin, P.; Wu, J.; Nie, X.; Zhang, G. Deposition of DLC films on the inner wall of U-type pipes by hollow cathode PECVD. *Diam. Relat. Mater.* **2021**, *114*, 108308.
16. Wei, X.; Shi, S.; Ning, C.; Lu, Z.; Zhang, G. Si-DLC films deposited by a novel method equipped with a co-potential auxiliary cathode for anti-corrosion and anti-wear application. *J. Mater. Sci. Technol.* **2022**, *109*, 114–128.
17. Wei, X.; Ning, C.; Lu, Z.; Zhang, G. Si and N incorporated hydrogenated diamond like carbon film with excellent performance for marine corrosion resistance. *Ceram. Int.* **2022**, *48*, 8440–8450.
18. Wei, X.; Chen, L.; Zhang, M.; Lu, Z.; Zhang, G. Effect of dopants (F, Si) material on the structure and properties of hydrogenated DLC film by plane cathode PECVD. *Diam. Relat. Mater.* **2020**, *110*, 108102.
19. Wang, X.; Sui, X.; Zhang, S.; Yan, M.; Yang, J.; Hao, J.; Liu, W. Effect of deposition pressures on uniformity, mechanical and tribological properties of thick DLC coatings inside of a long pipe prepared by PECVD method. *Surf. Coat. Technol.* **2019**, *375*, 150–157.
20. Yi, X.; Li, L.; Luo, S.; Lu, Q.; Gu, J.; Lei, N.; Huo, C. Self-enhanced plasma discharge effect in the deposition of diamond-like carbon films on the inner surface of slender tube. *Appl. Surf. Sci.* **2017**, *393*, 467–473.
21. Santos, N.; Mariano, S.; Ueda, M. Carbon films deposition as protective coating of titanium alloy tube using PIII&D system. *Surf. Coat. Technol.* **2019**, *375*, 164–170.
22. Ferrari, A.C.; Robertson, J. Interpretation of Raman spectra of disordered and amorphous carbon. *Phys. Rev. B* **2000**, *61*, 14095–14107.
23. Casiraghi, C.; Ferrari, A.C.; Robertson, J. Raman spectroscopy of hydrogenated amorphous carbons. *Phys. Rev. B* **2005**, *72*, 85401.
24. Casiraghi, C.; Piazza, F.; Ferrari, A.C.; Grambole, D.; Robertson, J. Bonding in hydrogenated diamond-like carbon by Raman spectroscopy. *Diam. Relat. Mater.* **2005**, *14*, 1098–1102.
25. Ferrari, A.C.; Robertson, J. Resonant Raman spectroscopy of disordered, amorphous, and diamondlike carbon. *Phys. Rev. B* **2001**, *64*, 75414.
26. Ferrari, A.C. Determination of bonding in diamond-like carbon by Raman spectroscopy. *Diam. Relat. Mater.* **2002**, *11*, 1053–1061.
27. Fayed, S.M.; Chen, D.; Li, S.; Zhou, Y.; Wang, H.; Sadawy, M.M. Corrosion behavior and passive stability of multilayer DLC-Si coatings. *Surf. Coat. Technol.* **2022**, *431*, 128001.
28. Fayed, S.M.; Gao, P.; Chen, D.; Li, S.; Zhou, Y.; Wang, H.; Sadawy, M.M. Corrosion inhibition characteristics of multilayer Si-DLC, phosphating and anodizing coatings deposited on 2024 Al alloy: A comparative study. *Diam. Relat. Mater.* **2021**, *117*, 108460.
29. Wang, J.; Pu, J.; Zhang, G.; Wang, L. Tailoring the structure and property of silicon-doped diamond-like carbon films by controlling the silicon content. *Surf. Coat. Technol.* **2013**, *59*, 321–320.
30. Bhowmick, S.; Banerji, A.; Lukitsch, M.J.; Alpas, A.T. The high temperature tribological behavior of Si, O containing hydrogenated diamond-like carbon (a-C:H/a-Si:O) coating against an aluminum alloy. *Wear* **2015**, *330*, 261–271.
31. Kolodziejczyk, L.; Niedzielski, P.; Clapa, M.; Jedrzejczak, A.; Szymanski, W. Influence of the process parameters on the characteristics of silicon-incorporated a-C:H:SiO_x coatings. Batory. *Surf. Coat. Technol.* **2015**, *271*, 112–118.
32. Wei, Y.L.; Huang, L.L.; Han, L.J.; Chen, Y.S. Corrosion resistance and surface biocompatibility of diamond-like carbon coating on AZ31D magnesium alloy. *Int. J. Surf. Sci. Eng.* **2016**, *10*, 101–115.
33. Hamdy, A.S. Electrochemical behavior of diamond-like-carbon coatings deposited on AlTiC (Al_2O_3 + TiC) ceramic composite substrate in HCl solution. *Electrochim. Acta* **2011**, *56*, 1554–1562.
34. Liu, L.; Wu, Z.; Cui, S.; An, X.; Ma, Z.; Shao, T.; Fu, R.K.Y.; Wang, R.; Lin, H.; Pan, F.; et al. Abrasion and erosion behavior of DLC-coated oil-well tubings in a heavy oil/sand environment. *Surf. Coat. Technol.* **2019**, *357*, 379–383.
35. Jacobsohn, L.G.; Schulze, R.K.; da Costa, M.E.H.M.; Nastasi, M. X-ray photoelectron spectroscopy investigation of boron carbide films deposited by sputtering. *Surf. Sci.* **2004**, *572*, 418–424.
36. Tamura, Y.; Zhao, H.; Wang, C.; Morina, A.; Neville, A. Interaction of DLC and B4C coatings with fully formulated oils in boundary lubrication conditions. *Tribol. Int.* **2016**, *93*, 666–680.